

See discussions, stats, and author profiles for this publication at: <https://www.researchgate.net/publication/275222615>

# Direct Fabrication of Au/Pd(II) Colloidal Core–Shell Nanoparticles by Pulsed Laser Ablation of Gold in PdCl<sub>2</sub> Solution

ARTICLE *in* THE JOURNAL OF PHYSICAL CHEMISTRY C · APRIL 2015

Impact Factor: 4.77 · DOI: 10.1021/jp512582q

---

READS

50

## 4 AUTHORS, INCLUDING:



Zahra Sheykhifard

Shahid Beheshti University

2 PUBLICATIONS 0 CITATIONS

[SEE PROFILE](#)



Hadi Salamati

Isfahan University of Technology

129 PUBLICATIONS 863 CITATIONS

[SEE PROFILE](#)

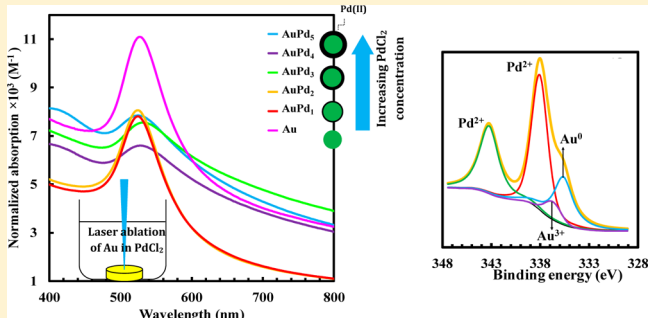
# Direct Fabrication of Au/Pd(II) Colloidal Core-Shell Nanoparticles by Pulsed Laser Ablation of Gold in $\text{PdCl}_2$ Solution

Zahra Sheykhanifard,<sup>†</sup> Mehdi Ranjbar,<sup>\*,†</sup> Hossein Farrokhpour,<sup>‡</sup> and Hadi Salamat<sup>†</sup>

<sup>†</sup>Department of Physics and <sup>‡</sup>Department of Chemistry, Isfahan University of Technology, Isfahan, Iran, 8415683111

**ABSTRACT:** In this study, Au/Pd(II) core-shell colloidal nanoparticles (NPs) were prepared by pulsed laser (Nd:YAG,  $\lambda = 1064 \text{ nm}$ ) ablation synthesis in solution (LASiS) of gold target in  $\text{PdCl}_2$  solution of different concentrations. From X-ray diffraction, metallic Au, PdO, or  $\text{PdCl}_2$  crystal phases were obtained in this process. Surface plasmon resonance investigations, by means of UV-vis spectrophotometer, revealed damping of Au peak by increasing  $\text{PdCl}_2$  concentration. Transmission electron microscope showed the bimetallic particles are spherical core Au NPs covered by a Pd(II) shell whose thickness is dependent on  $\text{PdCl}_2$  concentration. X-ray photoelectron spectroscopy was used for surface chemical analysis.

On the basis of the results from the previously described measurements, a mechanism for Au/Pd(II) core-shell formation was given.



## 1. INTRODUCTION

In recent years, noble-metal NPs suspended in a solution have spectacular development because of their peculiar physical and chemical properties such as interesting optical, catalytic, electronic, and magnetic properties that are distinctly different and unique from those of bulk sample.<sup>1–17</sup> These advantages are related to quantum size effects on the nanoscale with respect to bulk samples and to the enhancement of surface properties due to large surface/volume ratio.<sup>16–18</sup> Various effects that influence the new properties include the emergence of electronic or atom-packing shell structures, along with fundamentally altered interactions among the nanocrystals.<sup>16</sup>

Gold NPs are probably the most attractive noble-metals nanostructure because of their unique and interesting physical and chemical properties.<sup>13–16</sup> Gold has adjustable optical absorption, chemical stability, and nontoxicity properties and has application in surface-enhanced Raman scattering (SERS),<sup>19,20</sup> surface plasmon resonance (SPR),<sup>21</sup> nonlinear optical (NLO) properties,<sup>22</sup> and quantized charging effects.<sup>23</sup>

Combining the physical–chemical properties of different metals in a single nanostructure would be useful in various applications.<sup>24</sup> In this regard, palladium NPs are widely used in various reactions, such as catalytic converting,<sup>25–27</sup> and it is well known that adding a second metallic component to produce bimetallic NPs enhances the activity, selectivity, and stability of pure metal catalysts.<sup>5,18</sup> Among the developed structures, core–shell Pd-based materials not only demonstrate high catalytic activity, stability, and durability but also provide a suitable form to understand the interaction between the core nanoparticle and Pd shell.<sup>28</sup> Catalytic properties of bimetallic NPs greatly depend on their structure (e.g., alloy and core–shell structure) and surface composition.<sup>29–31</sup> Among them, core–shell nanostructures have attracted more attention because shell addition can enhance the

stability and dispersibility of bare core particles and modify or enhance their properties.<sup>15</sup>

Au–Pd core–shell NPs are reported to show excellent electrochemical properties in fuel cells.<sup>32</sup> For example, the turnover rate for the reaction between dihydrogen and dioxygen to form water is considerably greater over Au–Pd than over pure Pd catalyst.<sup>33</sup> In Au–Pd systems, the electronic interaction between the two elements gives an enhancement to the catalytic efficiency of Pd, leading to great potential applications in Pd and Au reactions.<sup>5</sup> Supported Au–Pd bimetallic catalysts have been used in some important reactions, such as hydrodesulfurization<sup>34</sup> or hydrodechlorination<sup>35</sup> of the fuel oil, vinyl acetate synthesis,<sup>36</sup> oxidation of carbon monoxide,<sup>37</sup> methane and ethanol,<sup>38</sup> liquid selective oxidation of organic compounds,<sup>39</sup> direct oxidation of hydrogen into hydrogen peroxide,<sup>40</sup> hydrogenation of acetylene,<sup>41</sup> aromatics,<sup>42</sup> and the oxidation of alcohols to aldehydes with  $\text{O}_2$ .<sup>7</sup> PdO has shown good combustion activity, methane activity, and oxidation of volatile organic compounds.<sup>43–46</sup> These properties may be improved in conjunction with noble metals like Au nanoparticles. Reduction of PdO to Pd for the formation of Au/Pd nanoparticles is very easy, for example, by using hydrogen gas.<sup>47</sup>

Different methods have been reported so far for the synthesis of Au–Pd core–shell NPs involving one-pot coreduction,<sup>48</sup> two-step seed-mediated growth method,<sup>49</sup> sonochemical,<sup>33</sup>  $\gamma$ -irradiation of a mixed solution of  $\text{Au}^{3+}$  and  $\text{Pd}^{2+}$  ions,<sup>33,50</sup> electron beam deposition,<sup>26</sup> chemical reduction,<sup>2,26</sup> polyol process,<sup>51</sup> solvent extraction/reduction,<sup>52</sup> and electrolysis of bulk.<sup>53</sup> These synthesis methods can be divided into successive

Received: December 17, 2014

Revised: April 5, 2015

Published: April 6, 2015

and simultaneous categories. The simultaneous method proceeds with the precursors of the two metals present in a same reaction system, and the successive method involves reducing ions of shell on the surface of the preformed core particles.<sup>9</sup> Recently, we have synthesized core-shell NPs of Pd/WO<sub>3</sub> and Pd/Ag successfully by adding PdCl<sub>2</sub> solution into WO<sub>3</sub> and Ag NPs preformed via pulsed laser ablation in DI water.<sup>26,54</sup> In the latter case, for example, it has been observed that core-shell NPs of Ag/Pd are generated in a successive approach and the SPR peaks of the Ag NPs were extinguished after the addition PdCl<sub>2</sub>. Indeed, because the reduction potential for metallic phase formation in the half-reaction of reduction palladium is more positive than that of Ag, the probability of Pd to be reduced is high enough to form a Pd shell on cores of Ag NPs; however, this is not the case of Au/Pd system because Pd is hardly reduced by Au. Therefore, to produce Au/Pd NPs by LASiS method, we used, in this report, a simultaneous approach in which laser ablation of Au was performed in PdCl<sub>2</sub> solution in water instead of pure water. We found that Au/Pd(II) core-shell NPs can be obtained by this single-step method.

The method of LASiS is a new way of carrying out the synthesis of noble-metal NPs that does not need stabilizing molecules or other chemicals and has been proven to provide an efficient approach for preparing various nanoscale materials.<sup>2</sup> Previously researchers could produce individual Au and Ag NPs in various liquid environments such as acetone, ethanol,<sup>55</sup> water,<sup>56</sup> alkanes,<sup>57</sup> and salt solution such NaCl.<sup>58</sup> In this method, by irradiating target with a pulsed laser beam, materials are directly removed from the target surface and propagate throughout the liquid. The ejected species undergo fast condensation and start to nucleate, and, as a result, nanoparticles are generated.<sup>59–61</sup> The LASiS technique provides some advantages over the other chemical methods of NPs synthesis, such as giving products with high purity due to direct interaction of laser beam with target surface, synthesis on a short time scale at ambient temperature, and a vast compositional range of both target and solvent.<sup>2</sup>

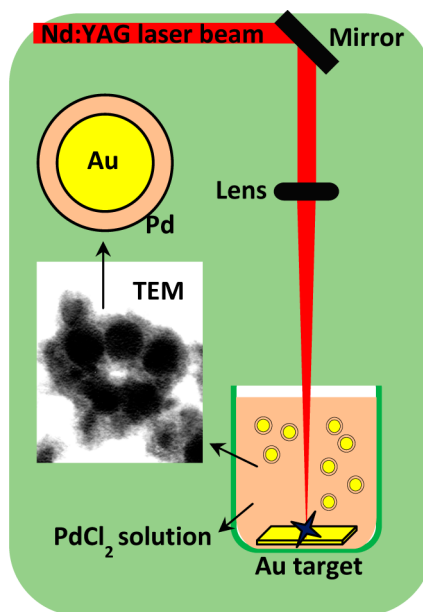


**Figure 1.** Schematic representation of experimental setup for preparing Au/Pd(II) bimetallic nanoparticles by LASiS of gold target in PdCl<sub>2</sub> solution.

**Table 1. Samples Name and Concentration of Components**

| sample                             | Au | AuPd <sub>1</sub> | AuPd <sub>2</sub> | AuPd <sub>3</sub> | AuPd <sub>4</sub> | AuPd <sub>5</sub> |
|------------------------------------|----|-------------------|-------------------|-------------------|-------------------|-------------------|
| Au concentration ( $\mu\text{M}$ ) | 46 | 104               | 106               | 75                | 57                | 73                |
| Pd concentration ( $\mu\text{M}$ ) | 0  | 6                 | 17                | 36                | 72                | 150               |

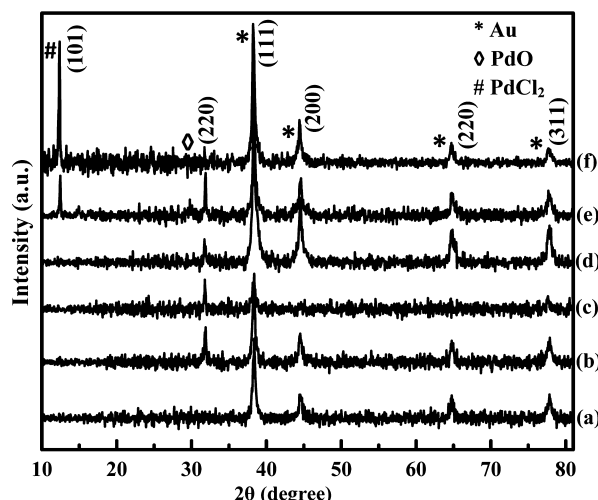


**Figure 2.** XRD patterns of different samples including (a) Au, (b) AuPd<sub>1</sub>, (c) AuPd<sub>2</sub>, (d) AuPd<sub>3</sub>, (e) AuPd<sub>4</sub>, and (f) AuPd<sub>5</sub>.

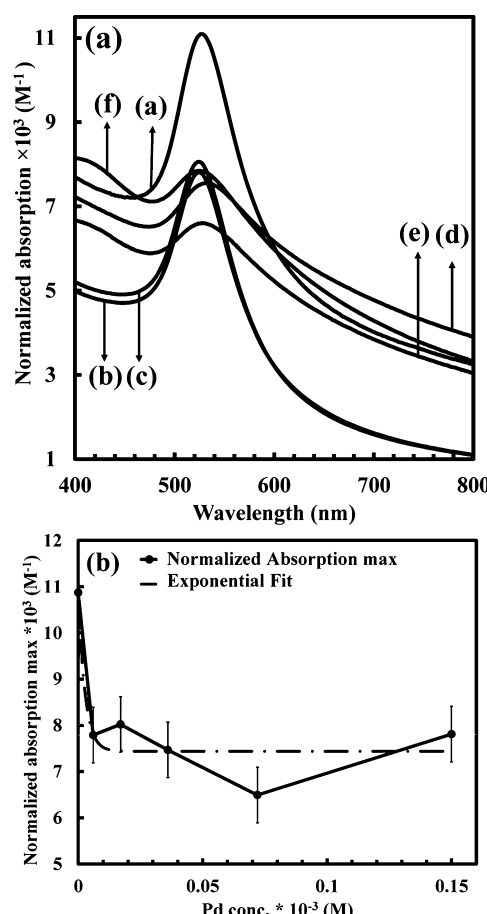


**Figure 3.** (a) Normalized optical absorption spectra of Au and Au/Pd(II) samples: (a) Au, (b) AuPd<sub>1</sub>, (c) AuPd<sub>2</sub>, (d) AuPd<sub>3</sub>, (e) AuPd<sub>4</sub>, and (f) AuPd<sub>5</sub>. (b) Curve of the normalized absorption maximum as a function of Pd concentration.

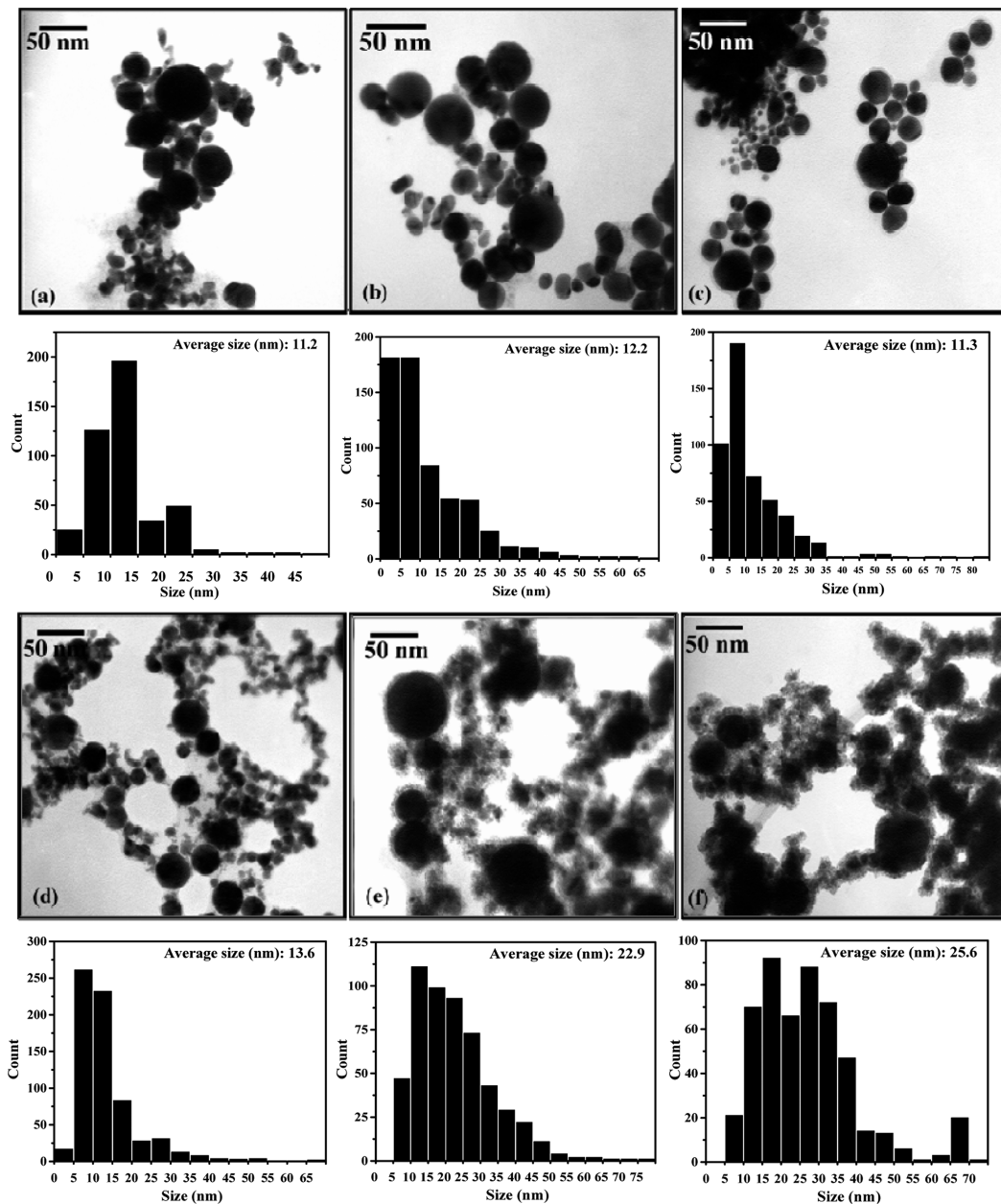


**Figure 4.** TEM images and corresponding size distribution histograms of Au and Au/Pd(II) samples: (a) Au, (b) AuPd<sub>1</sub>, (c) AuPd<sub>2</sub>, (d) AuPd<sub>3</sub>, (e) AuPd<sub>4</sub>, and (f) AuPd<sub>5</sub>.

We describe a method to prepare Au colloidal NPs in a solution containing a noble-metal salt solute by use of laser ablation on a Au metal plate immersed in the solution. The noble-metal salt ( $\text{PdCl}_2$ ) surrounds each nanoparticle and forms a nanoscale shell of palladium. The formation mechanism of Au/Pd(II) NPs in the solution was explored by changing the concentration of  $\text{PdCl}_2$  solution. The produced nanoparticles, observed by TEM, have core–shell structures. Other characterizations techniques involving XRD, UV-vis, and XPS were employed for investigation of structural, optical, and surface chemical investigations.

## 2. EXPERIMENTAL SECTION

The experimental setup is schematically shown in Figure 1. The main components of the system are a glass vessel containing solution, a mirror, and a convex lens for light direction control

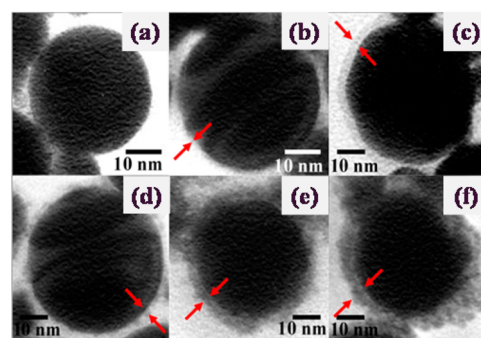


**Figure 5.** TEM images of one NPs of Au and Au/Pd(II) of samples: (a) Au, (b) AuPd<sub>1</sub>, (c) AuPd<sub>2</sub>, (d) AuPd<sub>3</sub>, (e) AuPd<sub>4</sub>, and (f) AuPd<sub>5</sub>.

and focusing. Laser ablation was performed by focusing the first harmonic of Nd:YAG laser pulse ( $\lambda = 1064$  nm,  $\tau = 5$  ns)

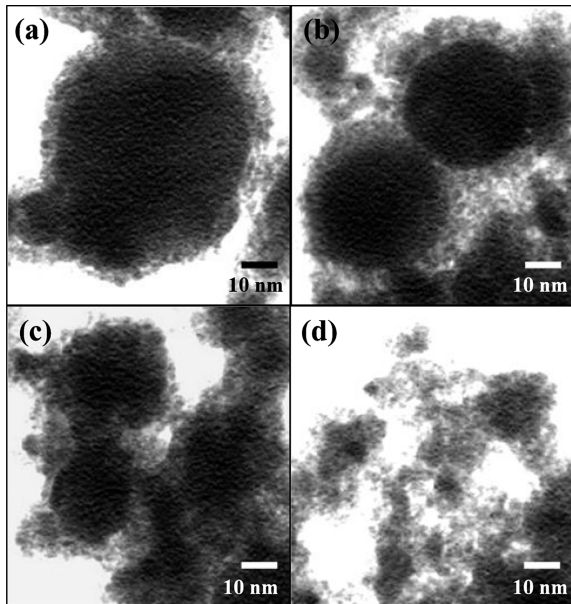


**Figure 6.** TEM images of AuPd<sub>5</sub> sample selected from different parts.

perpendicularly aligned to the target surface and operating at a repetition rate of 10 HZ and energy 360 mJ per pulse. For preparation of PdCl<sub>2</sub> solution, 0.02 g of PdCl<sub>2</sub> powder was dissolved in a mixture of 100 mL of DI water and 0.1 mL of HCl, followed by 1 h of sonication. PdCl<sub>2</sub> solutions with different concentrations were prepared by diluting the primary solution. Then, a gold plate with purity of 99.99% was fixed at the bottom of the glass vessel filled with 80 mL of the previously described PdCl<sub>2</sub> solution. Au/Pd(II) NPs with different composition and a pure Au as reference sample were prepared and named Au, AuPd<sub>1</sub>, AuPd<sub>2</sub>, AuPd<sub>3</sub>, AuPd<sub>4</sub>, and AuPd<sub>5</sub> (Table 1). Using inductively coupled plasma optical emission spectroscopy (ICP-OES) (Optima 7300 DV) analysis, the primary Au concentration was obtained to be 9.2, 20.7, 20.9, 14.9, 11.4, and 14.5 ppm for samples Au, AuPd<sub>1</sub>, AuPd<sub>2</sub>, AuPd<sub>3</sub>, AuPd<sub>4</sub>, and AuPd<sub>5</sub>, respectively. The crystalline structure of drop-casting samples was characterized using X-ray diffractometer (Philips EXPERTMPD) with Cu K $\alpha$  ( $\lambda = 0.154$  nm) radiation. The size and morphology of nanoparticles were observed on a Philips model CM120 TEM. XPS was done in an ESCA/AES system equipped with a concentric hemispherical analyzer (CHA, Specs model EA10 plus). Optical properties of samples (1 cm optical path length cell) were measured in the 190–1100 nm wavelength range using a Lambda 25 spectrophotometer (PerkinElmer).

### 3. RESULTS AND DISCUSSION

**3.1. XRD.** XRD patterns of drop-casting Au and Au/Pd(II) NPs of different compositions are shown in Figure 2. For samples Au, AuPd<sub>1</sub>, AuPd<sub>2</sub>, AuPd<sub>3</sub>, AuPd<sub>4</sub>, and AuPd<sub>5</sub>, each pattern comprises Au(111), Au(200), and Au(311) diffraction peaks corresponding to crystallographic orientations of cubic crystal structure of gold (JCPDS no. 00-001-1172). Except for sample Au, a diffraction peak exists at  $2\theta = 32^\circ$ , which is assigned to simple cubic PdO (220) orientation (JCPDS no. 00-046-1211), and an additional diffraction peak is clearly seen at  $2\theta = 12.3^\circ$  only for samples AuPd<sub>4</sub> and AuPd<sub>5</sub>, which is related to rhombohedral PdCl<sub>2</sub> phases (JCPDS no. 01-086-1888). No diffraction peaks of well-crystalline metallic Pd appeared in XRD patterns of samples, indicating that the metallic palladium phase

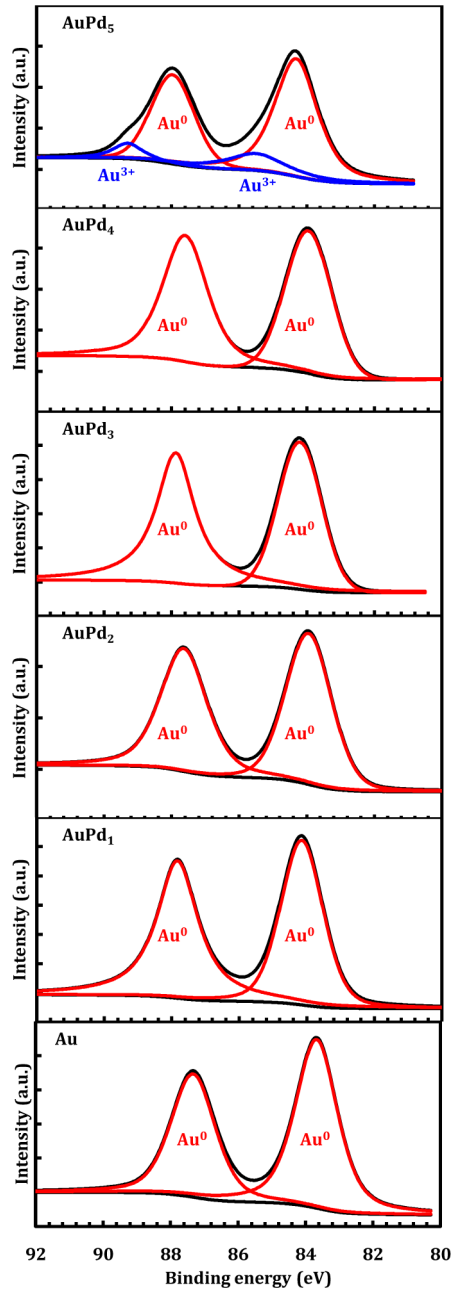


**Figure 7.** High-resolution XPS spectra of Au 4f core level of Au and Au/Pd(II) samples.

might exist in an amorphous phase or in the form of very small clusters.<sup>38</sup> Even though PdO is expected to have formed gradually after drop-casting in ambient air, the existence of PdO would be essentially associated with a possible chemical reaction between palladium salt solution and generated gold species either during or after the process of LASiS. This reaction's progress may be limited by the gold to palladium salt concentration ratio, and this is why we see PdCl<sub>2</sub> traces in XRD patterns when the solution concentration exceeds a certain level.

**3.2. Optical Properties.** The variation of SPR property of gold NPs produced by LASiS at each the PdCl<sub>2</sub> solution concentration was investigated by UV-vis absorption spectra. Figure 3a shows the normalized UV-vis absorption spectra of Au and Au/Pd(II) NPs samples. The optical absorption of a

Table 2. Au 4f Core-Level XPS of Au and Au/Pd(II) Samples

| sample            | XPS peak                                |            |   |                                |
|-------------------|---|------------|---|--------------------------------|
|                   | Au 4f <sub>7/2</sub> (Au <sup>0</sup> ) |            | Au 4f <sub>5/2</sub> (Au <sup>0</sup> ) |                                |
|                   | B.E. (eV)                               | fw hm (eV) | B.E. (eV)                               | fw hm (eV)                     |
| Au                | 83.7                                    | 1.5        | 87.3                                    | 1.5                            |
| AuPd <sub>1</sub> | 84.1                                    | 1.5        | 87.8                                    | 1.4                            |
| AuPd <sub>2</sub> | 83.9                                    | 1.6        | 87.7                                    | 1.6                            |
| AuPd <sub>3</sub> | 84.2                                    | 1.5        | 87.9                                    | 1.4                            |
| AuPd <sub>4</sub> | 83.9                                    | 1.6        | 87.6                                    | 1.6                            |
| AuPd <sub>5</sub> | 84.3                                    | 1.5        | 88.0                                    | 1.5                            |
|                   |   |            |   | 85.5      2      89.3      1.1 |

colloidal solution is a linear function of its concentration according to Beer–Lambert relation<sup>23,62</sup>

$$A = \epsilon cl \quad (1)$$

where  $A$  is absorption,  $\epsilon$  is absorption coefficient,  $c$  is concentration of solution, and  $l$  is cell thickness (1.0 cm in this study). We normalized, therefore, the absorption spectra to their gold concentrations. In this Figure, each curve exhibits one intense SPR peak with center at  $\sim 530$  nm which is characteristic of gold colloidal NPs.<sup>7,63</sup> The normalized absorption maximum is plotted as a function of Pd molarity in Figure 3b. By increasing Pd content, the normalized SPR intensity demonstrates a reducing trend, and it was tried to fit the plot to an exponential function. Although SPR is often affected by different factors such as nature, size, shape, and aggregation of nanoparticles<sup>17,30,58,63–65</sup> but because it is a surface phenomenon, damping of the SPR peaks is also attributed to formation of a passivating layer of palladium over the gold NPs. A possible description to explain this effect may be as follows: damping of SPR is due to the formation of PdO or PdCl<sub>2</sub> shells, and their imaginary part of the optical constant is responsible for SPR damping.

**3.3. TEM.** The size and shape of the Au and Au/Pd(II) NPs were studied on TEM. Figure 4a–f shows the TEM images and corresponding size distribution histogram of Au and Au/Pd(II) samples. The TEM image of pure Au NPs (part a) consists of many spherical particles of different sizes. The size distribution histogram of this sample reveals that the average particle size is  $\sim 11.2$  nm. The formation of spherical NPs of noble metals by laser ablation method in liquid has been reported elsewhere.<sup>3,17,63,66–68</sup> For Au/Pd(II) NPs samples the spherical Au core is covered with a thin layer of Pd shell in which the Pd thickness increases with PdCl<sub>2</sub> concentration. The Pd shells are recognizable by different contrasts in TEM images because of difference in Au and Pd atomic numbers. The average total particle sizes (and standard deviations) are about 11.2 (7.2 nm), 12.2 (10.9 nm), 11.3 (9.3 nm), 13.6 (9.0 nm), 22.9 (11.4 nm), and 25.7 nm (11.2 nm) for Au, AuPd<sub>1</sub>, AuPd<sub>2</sub>, AuPd<sub>3</sub>, AuPd<sub>4</sub>, and AuPd<sub>5</sub> samples, respectively. Besides, the measured shell thicknesses are 0.9, 2.5, 3.7, 5.0, and 6.2 nm for AuPd<sub>1</sub>, AuPd<sub>2</sub>, AuPd<sub>3</sub>, AuPd<sub>4</sub>, and AuPd<sub>5</sub> samples, respectively. The sudden increase in total particles size for samples AuPd<sub>4</sub> (22.9 nm) and AuPd<sub>5</sub> (25.7 nm) is due to their thicker thickness as the shells are more visible in these two samples (Figure 5a–f). This observation is in agreement with the UV–vis spectra, where an exponential decrease in SPR absorption was observed.

In Figure 6a–d, for a specific sample(AuPd<sub>5</sub>) it was observed that by increasing Au core size Pd shell thickness decreases, which may be due to increasing surface activity with decrease in NP size. Therefore, smaller Au nanoparticles have much tendency for absorbing Pd atoms. From TEM images it can be concluded that the formation of Au/Pd(II) core–shell NPs, in

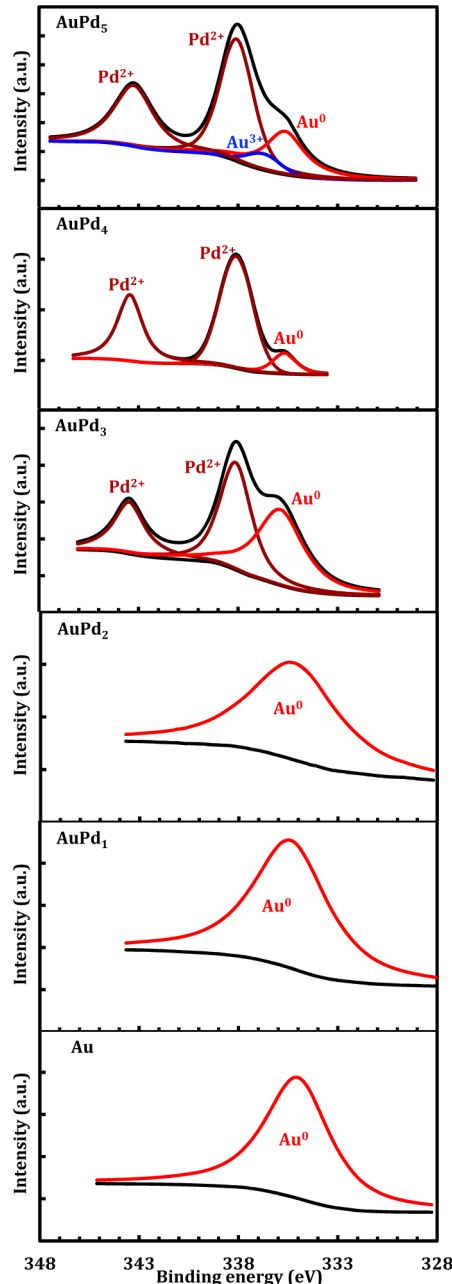


Figure 8. Pd 3d and Au 4d core-level XPS of Au and Au/Pd(II) samples.

our method, is possible and the PdCl<sub>2</sub> concentration is an effective parameter to control the Pd shell thickness.

**3.4. XPS.** To study the surface chemical compositions and investigation of Pd shells in Au/Pd(II) core–shell NPs in details,

Table 3. Au 4d and Pd 3d Core-Level XPS of Au and Au/Pd(II) Samples

| sample            | Au 4d <sub>5/2</sub> (Au <sup>0</sup> ) |            | Au 4d <sub>5/2</sub> (Au <sup>3+</sup> ) |            | Pd 3d <sub>5/2</sub> (Pd <sup>2+</sup> ) |            | Pd 3d <sub>3/2</sub> (Pd <sup>2+</sup> ) |            |
|-------------------|---|------------|--|------------|--|------------|--|------------|
|                   | B.E. (eV)                               | fw hm (eV) | B.E. (eV)                                | fw hm (eV) | B.E. (eV)                                | fw hm (eV) | B.E. (eV)                                | fw hm (eV) |
| Au                | 335                                     | 3.9        |  |            |  |            |  |            |
| AuPd <sub>1</sub> | 335.4                                   | 4.5        |  |            |  |            |  |            |
| AuPd <sub>2</sub> | 335.2                                   | 5.3        |  |            |  |            |  |            |
| AuPd <sub>3</sub> | 335.9                                   | 2.8        |  |            | 338.1                                    | 1.9        | 344.5                                    | 1.8        |
| AuPd <sub>4</sub> | 335.7                                   | 1.4        |  |            | 338.1                                    | 2.0        | 343.4                                    | 1.5        |
| AuPd <sub>5</sub> | 335.6                                   | 2.3        | 336.72                                   | 2          | 338.1                                    | 2.0        | 343.2                                    | 2.3        |

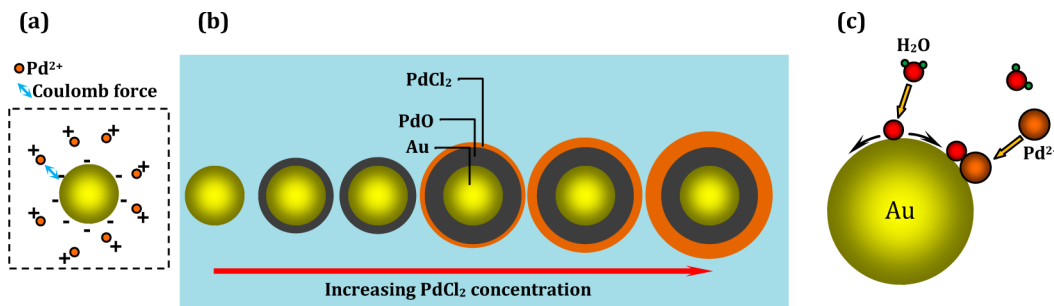


Figure 9. Schematic model for (a) attractive forces applied to the positive charges of the palladium ions, (b) core–shell NPs growth mechanism, and (c) PdO oxidation under the coexistence of moisture.

we performed chemical analysis of drop-casting samples using XPS. High-resolution XPS spectra of the samples Au, AuPd<sub>1</sub>, AuPd<sub>2</sub>, AuPd<sub>3</sub>, AuPd<sub>4</sub>, and AuPd<sub>5</sub> are shown in Figure 7. The peak positions and fwhm values are presented in Table 2. Au 4f spectra of all samples could be deconvoluted into one or two (only for sample AuPd<sub>5</sub>) spin–orbit doublets because the fwhm of initial peaks was broader in sample AuPd<sub>5</sub> compared with other samples. The spin–orbit splitting of Au 4f<sub>7/2</sub> and Au 4f<sub>5/2</sub> is ~3.6 eV. The Au 4f<sub>7/2</sub> and Au 4f<sub>5/2</sub> peaks have binding energy at about 84 and 87.5 eV, respectively, characteristic of Au<sup>0</sup>, and two extra peaks in sample AuPd<sub>5</sub> are located at binding energies of 85.49 and 89.29 eV, respectively, which are assigned to the presence of Au<sup>3+</sup> state.<sup>69–72</sup> For sample AuPd<sub>5</sub> the presence of Au<sup>3+</sup> states can be attributed to partial formation of gold chloride. The formation of AuCl<sub>3</sub> in laser ablation of gold in CHCl<sub>3</sub> has been reported elsewhere.<sup>73</sup> A positive shift was observed for binding energy Au 4f for Au/Pd(II) core–shell NPs with respect to pure Au NPs that is due to interaction between Au/Pd(II) core–shell NPs.<sup>38</sup> The increase in relative intensity of the Pd/Au with increasing palladium content is due to the increased palladium shell thickness, as was shown by TEM images (Figure 5).

High-resolution Pd 3d XPS spectra of samples Au and Au/Pd(II) are shown in Figure 8. The peak positions and fwhm values are presented in Table 3. It should be noted that the Pd 3d and Au 4f<sub>5/2</sub> core-level spectra overlap in the region of 328–348 eV. For sample Au and samples of low Pd content including AuPd<sub>1</sub> and AuPd<sub>2</sub>, no strong signal of Pd 3d can be observed, indicating very low concentration of palladium exist in contact with Au NPs, which was shown qualitatively on TEM images as well; however, for samples of higher Pd content, AuPd<sub>3</sub>, AuPd<sub>4</sub>, and AuPd<sub>5</sub>, there are Pd 3d<sub>5/2</sub> and Pd 3d<sub>3/2</sub> core-level peaks at about 338 and 344 eV, respectively. The peak positions are almost the same for all three samples. These peaks are related to Pd<sup>2+</sup> oxide states in PdO chemical composition.<sup>74,75</sup> Therefore, Pd 3d XPS spectra demonstrate that palladium is oxidized in the LASiS formation process of Au/Pd(II) NPs or after drop-casting in air. Moreover, it can be seen that the relative

XPS signal of Pd 3d increases by Pd content, which according to the TEM images of these core–shell structures, is due to the increase in Pd shell thickness. Indeed, XPS analysis is a surface-sensitive technique<sup>76</sup> and thus the signals incoming from a surface layer would dominate those of the beneath layer when a new surface layer develops over it. In addition to the Pd 3d doublet, the XPS peaks of Au 4d<sub>5/2</sub> that are located at binding energies of ~335.5 eV are observable in Figure 8. These peak positions reflect the presence of metallic Au, and the decomposing peak centered at 336.7 eV of sample AuPd<sub>5</sub> is related to the presence of Au<sup>3+</sup> state.

The surface concentration ratio of Pd/Au was estimated using the following relation<sup>69</sup> for Au/Pd(II) samples

$$\frac{C_{\text{Pd}}}{C_{\text{Au}}} = \frac{I_{\text{Pd}}/S_{\text{Pd}}}{I_{\text{Au}}/S_{\text{Au}}} \quad (2)$$

where C, I, and S are the elemental concentration, XPS peak area, and corresponding sensitivity factors. The relative surface ratio of C<sub>Pd</sub>/C<sub>Au</sub> for sample AuPd<sub>3</sub> is 0.8, which increases to about 3.2 and 3.3 for samples AuPd<sub>4</sub> and AuPd<sub>5</sub>, respectively. They are compared with C<sub>Pd</sub>/C<sub>Au</sub> from ICP measurements in Table 1, which indicates that palladium was enriched on the surface of gold NPs. This suggests that gold would be at the core of the bimetallic structure and palladium is deposited or enriched on the surface.<sup>38,69</sup>

#### 4. MECHANISM

XRD indicated that Au and PdO crystalline phases exist at each the PdCl<sub>2</sub> concentrations with solid PdCl<sub>2</sub> rhombohedra phase appearing at high concentrations. Moreover, from TEM images it can be inferred that a uniform shell of palladium surrounds first the spherical Au NPs while shells get porous morphology with much higher thickness at higher concentrations. Indeed, noble-metal nanoparticles have negative surface charges that can apply attractive forces to positive charges of palladium ions (Pd<sup>2+</sup>). Because of this driving force free palladium ions are accumulated

over the gold NPs (Figure 9a). On the basis of our observations and XPS findings about the presence of PdO or  $\text{PdCl}_2$  ( $\text{Pd}^{2+}$ ) surface composition, one can propose a model for the growth mechanism. In this model, which is shown schematically in Figure 9b, following the coulomb-induced diffusion of palladium ions, they surround the Au NPs and form a thin shell of PdO through a complex reduction reaction. The surface of Au cores is assumed to have a deterministic role for an ability to trap Pd ions owing to surface negative charges. The formation of Pd shell passivates it and prevents more particles to be trapped. At small concentrations of LASiS solution,  $\text{Pd}(\text{II})$  ions are completely consumed by Au NPs, while at high concentrations the extra  $\text{PdCl}_2$  salt is recovered in drop-casting process as a second shell over the first PdO shell. Okumura et al. have reported the role of moisture in catalytic activity of gold NPs for CO oxidation and described an oxidation model in which one of its process steps is activation of oxygen ions, dissociated, namely, from water, over the gold.<sup>77</sup> Moreover, oxidation during laser ablation in water has been reported in literature.<sup>78–80</sup> Using this consideration, palladium ions react with activated oxygen and form a PdO shell. This is a possible mechanism for when oxidation of palladium takes place in solution but not after drop-casting procedure. A schematic model that summarizes the discussion is shown in Figure 9c.

## 5. CONCLUSIONS

In summary, a single-step synthesis of Au/Pd(II) core–shell NPs by laser ablation of gold target in  $\text{PdCl}_2$  solution was presented. The SPR absorption peak of Au was observed to damp exponentially with  $\text{PdCl}_2$  concentration. The particle average size increases with the solution concentration due to increase in shell thickness. From XRD and XPS, the shell comprised PdO and even remained  $\text{PdCl}_2$  from the salt recovery. The surface activity of gold particles is believed to play a role in the accumulation of palladium ions and the formation shell. The possible oxidation of palladium was attributed to the formation of active oxygen atoms over gold form water dissociation that are able to react with palladium to form PdO.

## AUTHOR INFORMATION

### Corresponding Author

\*E-mail: ranjbar@cc.iut.ac.ir.

### Notes

The authors declare no competing financial interest.

## REFERENCES

- (1) Liu, F.; Wechsler, D.; Zhang, P. Alloy-Structure-Dependent Electronic Behavior and Surface Properties of Au–Pd Nanoparticles. *Chem. Phys. Lett.* **2008**, *461*, 254–259.
- (2) Amendola, V.; Meneghetti, M. Laser Ablation Synthesis in Solution and Size Manipulation of Noble Metal Nanoparticles. *Phys. Chem. Chem. Phys.* **2009**, *11*, 3805–3821.
- (3) Darroudi, M.; Ahmad, M.; Zamiri, R.; Abdullah, A.; Ibrahim, N.; Sadrolhosseini, A. Time-Dependent Preparation of Gelatin-Stabilized Silver Nanoparticles by Pulsed Nd: Yag Laser. *Solid State Sci.* **2011**, *13*, 520–524.
- (4) Liao, J.; Zhang, Y.; Yu, W.; Xu, L.; Ge, C.; Liu, J.; Gu, N. Linear Aggregation of Gold Nanoparticles in Ethanol. *Colloids Surf., A* **2003**, *223*, 177–183.
- (5) Annan, W.; Qing, P.; Yadong, L. Rod-Shaped Au–Pd Core–Shell Nanostructures. *Chem. Mater.* **2011**, *23*, 3217–3222.
- (6) Venkatesan, P.; Santhanakshmi, J. Core–Shell Bimetallic Au–Pd Nanoparticles: Synthesis, Structure, Optical and Catalytic Properties. *Nanosci. Nanotechnol.* **2011**, *1*, 43–47.
- (7) Akita, T.; Hiroki, T.; Tanaka, S.; Kojima, T.; Kohyama, M.; Iwase, A.; Hori, F. Analytical Tem Observation of Au–Pd Nanoparticles Prepared by Sonochemical Method. *Catal. Today* **2008**, *131*, 90–97.
- (8) Toshima, N. Core/Shell-Structured Bimetallic Nanocluster Catalysts for Visible-Light-Induced Electron Transfer. *Pure Appl. Chem.* **2000**, *72*, 317–325.
- (9) Mandal, M.; Kundu, S.; Ghosh, S. K.; Pal, T. Micelle-Mediated Uv-Photoactivation Route for the Evolution of Pdcore-Aushell and Pdcore-Agshell Bimetallics from Photogenerated Pd nanoparticles. *J. Photochem. Photobiol., A* **2004**, *167*, 17–22.
- (10) Chen, Y.-H.; Tseng, Y.-H.; Yeh, C.-S. Laser-Induced Alloying Au–Pd and Ag–Pd Colloidal Mixtures: The Formation of Dispersed Au/Pd and Ag/Pd Nanoparticles. *J. Mater. Chem.* **2002**, *12*, 1419–1422.
- (11) Mirdamadi-Esfahani, M.; Mostafavi, M.; Keita, B.; Nadjo, L.; Kooyman, P.; Remita, H. Bimetallic Au–Pt Nanoparticles Synthesized by Radiolysis: Application in Electro-Catalysis. *Gold Bull.* **2010**, *43*, 49–56.
- (12) Horikoshi, S.; Serpone, N. *Microwaves in Nanoparticle Synthesis: Fundamentals and Applications*; John Wiley & Sons: Berlin, 2013; pp 1–5.
- (13) Wu, F.; Yang, Q. Ammonium Bicarbonate Reduction Route to Uniform Gold Nanoparticles and Their Applications in Catalysis and Surface-Enhanced Raman Scattering. *Nano Res.* **2011**, *4*, 861–869.
- (14) Stadnichenko, A.; Koschcheev, S.; Boronin, A. Oxidation of the Polycrystalline Gold Foil Surface and Xps Study of Oxygen States in Oxide Layers. *Moscow Univ. Chem. Bull.* **2007**, *62*, 343–349.
- (15) Zhang, J.; Post, M.; Veres, T.; Jakubek, Z. J.; Guan, J.; Wang, D.; Normandin, F.; Deslandes, Y.; Simard, B. Laser-Assisted Synthesis of Superparamagnetic Fe@Au Core–Shell Nanoparticles. *J. Phys. Chem. B* **2006**, *110*, 7122–7128.
- (16) Abdelsayed, V.; Glaspell, G.; Nguyen, M.; Howe, J. M.; El-Shall, M. S. Laser Synthesis of Bimetallic Nanoalloys in the Vapor and Liquid Phases and the Magnetic Properties of Pdm and Pt<sub>m</sub> Nanoparticles (M=Fe, Co and Ni). *Faraday Discuss.* **2008**, *138*, 163–180.
- (17) Cristoforetti, G.; Pitzalis, E.; Spinello, R.; Ishak, R.; Muniz-Miranda, M. Production of Palladium Nanoparticles by Pulsed Laser Ablation in Water and Their Characterization. *J. Phys. Chem. C* **2010**, *115*, 5073–5083.
- (18) Baletto, F.; Mottet, C.; Ferrando, R. Time Evolution of Ag–Cu and Ag–Pd Core–Shell Nanoclusters. *Eur. Phys. J. D* **2003**, *24*, 233–236.
- (19) Cao, Y. C.; Jin, R.; Mirkin, C. A. Nanoparticles with Raman Spectroscopic Fingerprints for DNA and RNA Detection. *Science* **2002**, *297*, 1536–1540.
- (20) Ringe, E.; Zhang, J.; Langille, M. R.; Sohn, K.; Cobley, C.; Au, L.; Xia, Y.; Mirkin, C. A.; Huang, J.; Marks, L. D. Effect of Size, Shape, Composition, and Support Film on Localized Surface Plasmon Resonance Frequency: A Single Particle Approach Applied to Silver Bipyramids and Gold and Silver Nanocubes. *MRS Proc.* **2009**, *1208*, 1208–1210.
- (21) Kim, K. Y. Application of Surface Plasmon Resonance Based Metal Nanoparticles. *Plasmonics: Princ. Appl.* **2012**, 283–312.
- (22) Klar, T.; Perner, M.; Grosse, S.; Von Plessen, G.; Spirk, W.; Feldmann, J. Surface-Plasmon Resonances in Single Metallic Nanoparticles. *Phys. Rev. Lett.* **1998**, *80*, 4249–4252.
- (23) Liu, X.; Atwater, M.; Wang, J.; Huo, Q. Extinction Coefficient of Gold Nanoparticles with Different Sizes and Different Capping Ligands. *Colloids Surf., B* **2007**, *58*, 3–7.
- (24) Amendola, V.; Scaramuzza, S.; Agnoli, S.; Polizzi, S.; Meneghetti, M. Strong Dependence of Surface Plasmon Resonance and Surface Enhanced Raman Scattering on the Composition of Au–Fe Nanoalloys. *Nanoscale* **2014**, *6*, 1423–1433.
- (25) Kim, J.-H.; Chung, H.-W.; Lee, T. R. Preparation and Characterization of Palladium Shells with Gold and Silica Cores. *Chem. Mater.* **2006**, *18*, 4115–4120.
- (26) Mottaghi, N.; Ranjbar, M.; Farrokhpour, H.; Khoshouei, M.; Khoshouei, A.; Kameli, P.; Salamat, H.; Tabrizchi, M.; Jalilian-Nosrati, M. Ag/Pd Core–Shell Nanoparticles by a Successive Method: Pulsed Laser Ablation of Ag in Water and Reduction Reaction of  $\text{PdCl}_2$ . *Appl. Surf. Sci.* **2014**, *292*, 892–897.

- (27) Nutt, M. O.; Heck, K. N.; Alvarez, P.; Wong, M. S. Improved Pd-on-Au Bimetallic Nanoparticle Catalysts for Aqueous-Phase Trichloroethene Hydrodechlorination. *Appl. Catal., B* **2006**, *69*, 115–125.
- (28) Hsu, C.; Huang, C.; Hao, Y.; Liu, F. Au/Pd Core–Shell Nanoparticles for Enhanced Electrocatalytic Activity and Durability. *Electrochim. Commun.* **2012**, *23*, 133–136.
- (29) Ferrer, D.; Torres-Castro, A.; Gao, X.; Sepulveda-Guzman, S.; Ortiz-Mendez, U.; Jose-Yacaman, M. Three-Layer Core/Shell Structure in Au-Pd Bimetallic Nanoparticles. *Nano Lett.* **2007**, *7*, 1701–1705.
- (30) Suo, Y.; Hsing, I. Synthesis of Bimetallic Pdau Nanoparticles for Formic Acid Oxidation. *Electrochim. Acta* **2011**, *56*, 2174–2183.
- (31) Alayoglu, S.; Nilekar, A. U.; Mavrikakis, M.; Eichhorn, B. Ru–Pt Core–Shell Nanoparticles for Preferential Oxidation of Carbon Monoxide in Hydrogen. *Nat. Mater.* **2008**, *7*, 333–338.
- (32) Hsu, C.; Huang, C.; Hao, Y.; Liu, F. Au/Pd Core–Shell Nanoparticles with Varied Hollow Au Cores for Enhanced Formic Acid Oxidation. *Nanoscale Res. Lett.* **2013**, *8*, 1–7.
- (33) Remita, H.; Etcheberry, A.; Belloni, J. Dose Rate Effect on Bimetallic Gold–Palladium Cluster Structure. *J. Phys. Chem. B* **2003**, *107*, 31–36.
- (34) Venezia, A.; La Parola, V.; Deganello, G.; Pawelec, B.; Fierro, J. Synergetic Effect of Gold in Au/Pd Catalysts During Hydrodesulfurization Reactions of Model Compounds. *J. Catal.* **2003**, *215*, 317–325.
- (35) Heck, K. N.; Nutt, M. O.; Alvarez, P.; Wong, M. S. Deactivation Resistance of Pd/Au Nanoparticle Catalysts for Water-Phase Hydrodechlorination. *J. Catal.* **2009**, *267*, 97–104.
- (36) Chen, M.; Luo, K.; Wei, T.; Yan, Z.; Kumar, D.; Yi, C.-W.; Goodman, D. The Nature of the Active Site for Vinyl Acetate Synthesis over Pd–Au. *Catal. Today* **2006**, *117*, 37–45.
- (37) Venezia, A.; Liotta, L.; Pantaleo, G.; La Parola, V.; Deganello, G.; Beck, A.; Koppány, Z.; Frey, K.; Horvath, D.; Guczi, L. Activity of  $\text{SiO}_2$  Supported Gold–Palladium Catalysts in Co Oxidation. *Appl. Catal., A* **2003**, *251*, 359–368.
- (38) Suo, Z.; Ma, C.; Jin, M.; He, T.; An, L. The Active Phase of Au–Pd/ $\text{Al}_2\text{O}_3$  for Co Oxidation. *Catal. Commun.* **2008**, *9*, 2187–2190.
- (39) Enache, D. I.; Barker, D.; Edwards, J. K.; Taylor, S. H.; Knight, D. W.; Carley, A. F.; Hutchings, G. J. Solvent-Free Oxidation of Benzyl Alcohol Using Titania-Supported Gold–Palladium Catalysts: Effect of Au–Pd Ratio on Catalytic Performance. *Catal. Today* **2007**, *122*, 407–411.
- (40) Enache, D. I.; Edwards, J. K.; Landon, P.; Solsona-Espriu, B.; Carley, A. F.; Herzing, A. A.; Watanabe, M.; Kiely, C. J.; Knight, D. W.; Hutchings, G. J. Solvent-Free Oxidation of Primary Alcohols to Aldehydes Using Au-Pd/TiO<sub>2</sub> Catalysts. *Science* **2006**, *311*, 362–365.
- (41) Lee, Y. W.; Kim, M.; Kim, Z. H.; Han, S. W. One-Step Synthesis of Au@Pd Core–Shell Nanoctahedron. *J. Am. Chem. Soc.* **2009**, *131*, 17036–17037.
- (42) Pawelec, B.; Venezia, A.; La Parola, V.; Cano-Serrano, E.; Campos-Martin, J.; Fierro, J. AuPd Alloy Formation in Au-Pd/ $\text{Al}_2\text{O}_3$  Catalysts and Its Role on Aromatics Hydrogenation. *Appl. Surf. Sci.* **2005**, *242*, 380–391.
- (43) McCarty, J. G. Kinetics of Pdo Combustion Catalysis. *Catal. Today* **1995**, *26*, 283–293.
- (44) Fujimoto, K. I.; Ribeiro, F. H.; Avalos-Borja, M.; Iglesia, E. Structure and Reactivity of Pdo/ZrO<sub>2</sub> Catalysts for Methane Oxidation at Low Temperatures. *J. Catal.* **1998**, *179*, 431–442.
- (45) Farrauto, R. J.; Lampert, J. K.; Hobson, M. C.; Waterman, E. M. Thermal Decomposition and Reformation of Pdo Catalysts; Support Effects. *Appl. Catal., B* **1995**, *6*, 263–270.
- (46) Cordi, E. M.; Falconer, J. L. Oxidation of Volatile Organic Compounds on Al<sub>2</sub>O<sub>3</sub>, Pd/Al<sub>2</sub>O<sub>3</sub>, and Pdo/Al<sub>2</sub>O<sub>3</sub> Catalysts. *J. Catal.* **1996**, *162*, 104–117.
- (47) Su, S. C.; Carstens, J. N.; Bell, A. T. A Study of the Dynamics of Pd Oxidation and Pdo Reduction by H<sub>2</sub> and CH<sub>4</sub>. *J. Catal.* **1998**, *176*, 125–135.
- (48) Kuai, L.; Yu, X.; Wang, S.; Sang, Y.; Geng, B. Au-Pd Alloy and Core–Shell Nanostructures: One-Pot Coreduction Preparation, Formation Mechanism, and Electrochemical Properties. *Langmuir* **2012**, *28*, 7168–7173.
- (49) Ding, Y.; Fan, F.; Tian, Z.; Wang, Z. L. Atomic Structure of Au-Pd Bimetallic Alloyed Nanoparticles. *J. Am. Chem. Soc.* **2010**, *132*, 12480–12486.
- (50) Mizukoshi, Y.; Fujimoto, T.; Nagata, Y.; Oshima, R.; Maeda, Y. Characterization and Catalytic Activity of Core–Shell Structured Gold/Palladium Bimetallic Nanoparticles Synthesized by the Sonochemical Method. *J. Phys. Chem. B* **2000**, *104*, 6028–6032.
- (51) Mandal, S.; Mandale, A. B.; Sastry, M. Keggin Ion-Mediated Synthesis of Aqueous Phase-Pure Au@Pd and Au@Pt Core–Shell Nanoparticles. *J. Mater. Chem.* **2004**, *14*, 2868–2871.
- (52) Esumi, K.; Shiratori, M.; Ishizuka, H.; Tano, T.; Torigoe, K.; Meguro, K. Preparation of Bimetallic Palladium–Platinum Colloids in Organic Solvent by Solvent Extraction–Reduction. *Langmuir* **1991**, *7*, 457–459.
- (53) Reetz, M. T.; Helbig, W.; Quaiser, S. A. Electrochemical Preparation of Nanostructural Bimetallic Clusters. *Chem. Mater.* **1995**, *7*, 2227–2228.
- (54) Ranjbar, M.; Kalhori, H.; Mahdavi, S. New Gasochromic System: Nanoparticles in Liquid. *J. Nanopart. Res.* **2012**, *14*, 1–10.
- (55) Dolgaev, S.; Simakin, A.; Voronov, V.; Shafeev, G.; Bozon-Verduraz, F. Nanoparticles Produced by Laser Ablation of Solids in Liquid Environment. *Appl. Surf. Sci.* **2002**, *186*, 546–551.
- (56) Simakin, A.; Voronov, V.; Shafeev, G.; Brayner, R.; Bozon-Verduraz, F. Nanodisks of Au and Ag Produced by Laser Ablation in Liquid Environment. *Chem. Phys. Lett.* **2001**, *348*, 182–186.
- (57) Compagnini, G.; Scalisi, A.; Puglisi, O. Production of Gold Nanoparticles by Laser Ablation in Liquid Alkanes. *J. Appl. Phys.* **2003**, *94*, 7874–7877.
- (58) Bae, C. H.; Nam, S. H.; Park, S. M. Formation of Silver Nanoparticles by Laser Ablation of a Silver Target in NaCl Solution. *Appl. Surf. Sci.* **2002**, *197*, 628–634.
- (59) Yang, G. Laser Ablation in Liquids: Applications in the Synthesis of Nanocrystals. *Prog. Mater. Sci.* **2007**, *52*, 648–698.
- (60) Deniz, A. E.; Vural, H. A.; Ortaç, B.; Uyar, T. Gold Nanoparticle/Polymer Nanofibrous Composites by Laser Ablation and Electrospinning. *Mater. Lett.* **2011**, *65*, 2941–2943.
- (61) Sasaki, K.; Takada, N. Liquid-Phase Laser Ablation. *Pure Appl. Chem.* **2010**, *82*, 1317–1327.
- (62) Weingartner, E.; Saathoff, H.; Schnaiter, M.; Streit, N.; Bitnar, B.; Baltensperger, U. Absorption of Light by Soot Particles: Determination of the Absorption Coefficient by Means of Aethalometers. *J. Aerosol Sci.* **2003**, *34*, 1445–1463.
- (63) Solati, E.; Mashayekh, M.; Dorranian, D. Effects of Laser Pulse Wavelength and Laser Fluence on the Characteristics of Silver Nanoparticle Generated by Laser Ablation. *Appl. Phys. A: Mater. Sci. Process.* **2013**, *112*, 689–694.
- (64) Tseng, M. L.; Huang, Y.-W.; Hsiao, M.-K.; Huang, H. W.; Chen, H. M.; Chen, Y. L.; Chu, C. H.; Chu, N.-N.; He, Y. J.; Chang, C. M. Fast Fabrication of a Ag Nanostructure Substrate Using the Femtosecond Laser for Broad-Band and Tunable Plasmonic Enhancement. *ACS Nano* **2012**, *6*, 5190–5197.
- (65) Ashkarran, A. A.; Bayat, A. Surface Plasmon Resonance of Metal Nanostructures as a Complementary Technique for Microscopic Size Measurement. *Int. Nano Lett.* **2013**, *3*, 50–59.
- (66) Maciulevičius, M.; Vinčiūnas, A.; Brikas, M.; Butsen, A.; Tarasenka, N.; Tarasenko, N.; Račiukaitis, G. Pulsed-Laser Generation of Gold Nanoparticles with on-Line Surface Plasmon Resonance Detection. *Appl. Phys. A: Mater. Sci. Process.* **2013**, *111*, 289–295.
- (67) Mirghassemzadeh, N.; Ghamkhari, M.; Dorranian, D. Dependence of Laser Ablation Produced Gold Nanoparticles Characteristics on the Fluence of Laser Pulse. *Soft Nanosci. Lett.* **2013**, *3*, 101–106.
- (68) Kim, H. J.; Bang, I. C.; Onoe, J. Characteristic Stability of Bare Au-Water Nanofluids Fabricated by Pulsed Laser Ablation in Liquids. *Opt. Lasers Eng.* **2009**, *47*, 532–538.
- (69) Devarajan, S.; Bera, P.; Sampath, S. Bimetallic Nanoparticles: A Single Step Synthesis, Stabilization, and Characterization of Au–Ag, Au–Pd, and Au–Pt in Sol–Gel Derived Silicates. *J. Colloid Interface Sci.* **2005**, *290*, 117–129.

- (70) Klyushin, A. Y.; Rocha, T. C.; Hävecker, M.; Knop-Gericke, A.; Schlögl, R. A near Ambient Pressure Xps Study of Au Oxidation. *Phys. Chem. Chem. Phys.* **2014**, *16*, 7881–7886.
- (71) Takigawa, R.; Higurashi, E.; Suga, T.; Sawada, R. Low-Temperature Bonding of Laser Diode Chips on Si Substrates with Oxygen and Hydrogen Atmospheric-Pressure Plasma Activation. In *Electronic Packaging Technology & High Density Packaging 2009. ICEPT-HDP'09*; IEEE: Piscataway, NJ, 2009; pp 475–477.
- (72) Tsai, H.; Hu, E.; Perng, K.; Chen, M.; Wu, J.-C.; Chang, Y.-S. Instability of Gold Oxide  $\text{Au}_2\text{O}_3$ . *Surf. Sci.* **2003**, *537*, L447–L450.
- (73) Compagnini, G.; Scalisi, A. A.; Puglisi, O. Ablation of Noble Metals in Liquids: A Method to Obtain Nanoparticles in a Thin Polymeric Film. *Phys. Chem. Chem. Phys.* **2002**, *4*, 2787–2791.
- (74) Zemlyanov, D.; Aszalos-Kiss, B.; Kleimenov, E.; Teschner, D.; Zafeiratos, S.; Hävecker, M.; Knop-Gericke, A.; Schlögl, R.; Gabasch, H.; Unterberger, W. In Situ Xps Study of Pd (111) Oxidation. Part 1:2d Oxide Formation in  $10^{-3}$  Mbar  $\text{O}_2$ . *Surf. Sci.* **2006**, *600*, 983–994.
- (75) Monteiro, R.; Zemlyanov, D.; Storey, J.; Ribeiro, F. Turnover Rate and Reaction Orders for the Complete Oxidation of Methane on a Palladium Foil in Excess Dioxygen. *J. Catal.* **2001**, *199*, 291–301.
- (76) Aldea, N.; Marginean, P.; Rednic, V.; Pintea, S.; Barz, B.; Gluhoi, A.; Nieuwenhuys, B.; Xie, Y.; Aldea, F.; Neumann, M. Crystalline and Electronic Structure of Gold Nanoclusters Determined by Exafs, Xrd and Xps Methods. *J. Optoelectron. Adv. Mater.* **2007**, *9*, 1555–1560.
- (77) Okumura, M.; Tsubota, S.; Haruta, M. Vital Role of Moisture in the Catalytic Activity of Supported Gold Nanoparticles. *Angew. Chem., Int. Ed.* **2004**, *43*, 2129–2132.
- (78) Liu, Z.; Yuan, Y.; Khan, S.; Abdolvand, A.; Whitehead, D.; Schmidt, M.; Li, L. Generation of Metal-Oxide Nanoparticles Using Continuous-Wave Fibre Laser Ablation in Liquid. *J. Micromech. Microeng.* **2009**, *19*, 1–7.
- (79) Maneeratanasarn, P.; Van Khai, T.; Kim, S. Y.; Choi, B. G.; Shim, K. B. Synthesis of Phase-Controlled Iron Oxide Nanoparticles by Pulsed Laser Ablation in Different Liquid Media. *Phys. Status Solidi A* **2013**, *210*, 563–569.
- (80) Sasaki, T.; Shimizu, Y.; Koshizaki, N. Preparation of Metal Oxide-Based Nanomaterials Using Nanosecond Pulsed Laser Ablation in Liquids. *J. Photochem. Photobiol., A* **2006**, *182*, 335–341.